

Full Research Paper

Structural, Thermoanalytical and Molecular Modeling Studies on *N*-(3-hydroxypropyl) 3 α ,12 α -Dihydroxy-5 β -cholan-24-amide and Its Monohydrates

Arto Valkonen*, Erkki Kolehmainen, Manu Lahtinen, Elina Sievänen, Virpi Noponen, Minna Tolonen and Reijo Kauppinen

Department of Chemistry, University of Jyväskylä, PO. Box 35, FIN-40014 University of Jyväskylä, Finland

* Author to whom correspondence should be addressed; E-mail: arto.valkonen@jyu.fi

Received: 17 August 2007; in revised form: 9 September 2007/ Accepted: 12 September 2007 /

Published: 12 September 2007

Abstract: The synthetic method for preparing *N*-(3-hydroxypropyl) 3 α ,12 α -dihydroxy-5 β -cholan-24-amide can lead to formation of at least three different crystal forms – an anhydrous compound and two monohydrates. The structural and thermal properties of these forms have been characterized by ^{13}C -CP/MAS-NMR and IR spectroscopy, thermogravimetry, differential scanning calorimetry and by powder and single crystal x-ray crystallography. In addition, theoretical ^{13}C -NMR chemical shift calculations were also performed for the anhydrous compound and for the first monohydrate, starting from single crystal structures and the structures of these species have now been verified. The first monohydrate, $\text{C}_{27}\text{H}_{47}\text{NO}_4 \cdot \text{H}_2\text{O}$, crystallizes in orthorhombic space group $P2_12_12_1$ with cell parameters: $a = 7.1148(2)$, $b = 18.1775(5)$, $c = 20.1813(6)$, $Z = 4$.

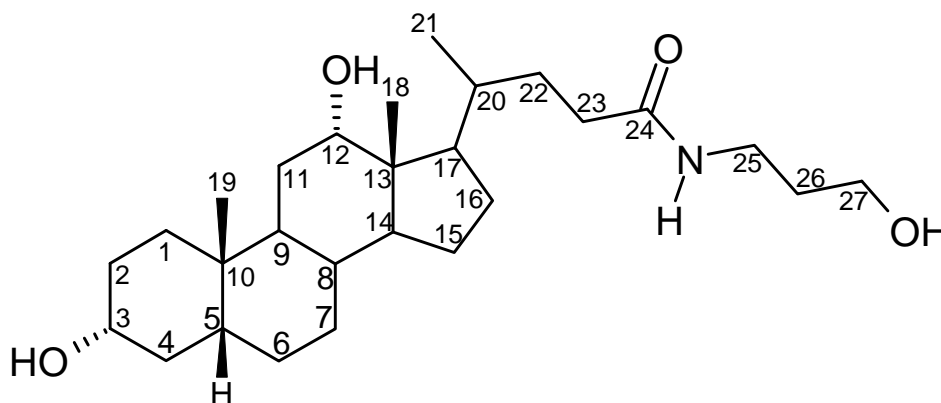
Keywords: Bile acids, ^{13}C -CP/MAS-NMR spectroscopy, crystallography, thermal analysis, solid state structure.

Introduction

Bile acids are widely applied in synthetic chemistry due to their enantiomeric purity, low cost and ready availability, combined with the different orientations and reactivity and varying number of their hydroxyl groups [1]. They are the natural ligands of enterohepatic circulation and are specifically recognized by intestinal and hepatic cells, which also makes them interesting compounds from the pharmacological point of view [2]. Some bile acid derivatives have an ability to act as enantiomer differentiating host molecules in inclusion processes [3,4]. Many bile acid derivatives are able to gel organic [e.g. 5-9] and aqueous solutions [e.g. 10-12]. Owing to these properties, bile acids are ideal building blocks for the construction of novel molecular and supramolecular assemblies for molecular recognition.

The investigation of the exact structures of bile acids and their derivatives in the solid state often proves to be complicated, because bile acids tend to precipitate out in forms unsuitable for single crystal X-ray structural studies. In our opinion, solid state NMR spectroscopy and crystallography [13,14] could provide some partial and novel solutions to these problems. We think that the ^{13}C -CP/MAS-NMR technique opens a direct and pharmaceutically very important scope for studies of bile acid derivatives in the solid state and when utilized together with TG, DSC, and powder x-ray diffraction, enables characterization of the structures, including polymorphs and pseudopolymorphs, of many bile acid derivatives, even in the absence of single crystal x-ray structures. As far as we know, there are no prior reports on ^{13}C -CP/MAS-NMR spectral studies of isolated bile acids or their derivatives, although a few reports on ^{13}C -CP/MAS-NMR studies of inclusion or binding interactions of bile acids, including interactions with barley β -D-glucan [15], carrot fiber [16], 2,3-dimethylbutadiene [17], ferrocene [18], and γ -valerolactone [19,20], can be found,

In a former study published by us [5] the synthesis and structures of *N*-(2-hydroxyethyl) and *N*-(3-hydroxypropyl) amides of 3α -hydroxy- 5β -cholan-24-oic (lithocholic, LCA) and $3\alpha,12\alpha$ -dihydroxy- 5β -cholan-24-oic (deoxycholic, DCA) acids as well as their gelation properties were discussed. Bile acid amidoalcohols have proven to be biologically interesting and active compounds. Some bile acid amidoalcohols are found to act as antimicrobials and antifungals [21] and could possibly be used in the treatment of inflammations and diseases [22-26]. These compounds are expected to have an effect on the ileal bile salt transport system [27]. One study shows that pathogenic strains could also biotransform human cholic acid (CA) derivatives to *N*-(2-hydroxyethyl) $3\alpha,7\alpha,12\alpha$ -trihydroxy- 5β -cholan-24-amide [28]. The ability of these compounds to gel organic solvents is also significant [5,8]. Due to these facts we feel that it is important to characterize the structure and function of these compounds more extensively. Solid state structures of these compounds are mainly unexplored. For example, from CSD database [29] only our crystal structure of *N*-(3-hydroxypropyl) $3\alpha,12\alpha$ -dihydroxy- 5β -cholan-24-amide [5] was found. In the present report we describe our new solid state structural findings, as well as thermoanalytical and modeling studies of *N*-(3-hydroxypropyl) $3\alpha,12\alpha$ -dihydroxy- 5β -cholan-24-amide (Scheme 1) and two of its monohydrates.

Scheme 1. General structure of *N*-(3-hydroxypropyl) 3 α ,12 α -dihydroxy-5 β -cholan-24-amide.

Results and Discussion

Solid state ^{13}C -CP/MAS-NMR spectra of the powdery solids **1–2**, the crystallized monohydrate **3**, as well as the anhydrous *N*-(3-hydroxypropyl) 3 α ,12 α -dihydroxy-5 β -cholan-24-amide (**4**) are presented in Figure 1. High quality spectra with sharp peaks proved these samples to be fairly crystalline. In our previous study [5] we reported the synthesis of solid **1** and the exact structure of crystalline material **4**. Solid **1** was precipitated by addition of the reaction mixture into large excess of water. From the spectra (Figure 1) it is observed that this precipitate (solid **1**) seems to contain forms **3** and **4**, in agreement with the previous findings [5], in which **1** was expected, according to crystallographic data, to be a mixture of two forms (**4** and an unidentified one). Unique resonances of both forms can be distinguished in the spectrum of **1** (Table 1). The double resonances for C18, C19 and C21 (methyls) in the spectrum fit nicely with the corresponding resonances of **3** and **4**. Also, the resonances of C27 (with a hydroxyl group attached to it) for **3** and **4** are found in the spectrum recorded for **1**. Two additional resonances of **1** at 41.6 and 39.3 ppm (Figure 1) correspond well with the resonances found for **3** (41.7 ppm) and for **4** (39.4 ppm), respectively. This gives an indication that the solid **1** is a mixture of the pure monohydrate **3** and the pure anhydrous form **4**.

Solid state NMR spectral data also proved the powdery solid **3** to be similar to the crystallized (from water/ethanol) sample of any of the powdery solids. The solid **2** shows the most complicated resonance pattern, which does not fit too well with the patterns of crystalline forms **3** and **4**. It seems to be a mixture of, at least, two different forms. The methyl signals on the shielded region of the spectra (Figure 1) of samples **3** and **4** are very sharp, while the deshielded carbonyl signals are broadened. This is most probably due to faster rotation of the methyls, and favourable relaxation properties, rather than different orientations or disorder of the amide side chains.

The solid **2** and the monohydrate **3** showed a broad signal at typical wavenumbers of O-H stretching absorption (around 3400 cm^{-1}), while in anhydrous compound **4** there were three resolved stretching signals, one for each OH group, at 3454 , 3410 , and 3316 cm^{-1} . Otherwise the IR analysis showed almost similar absorption behavior for all of the investigated forms.

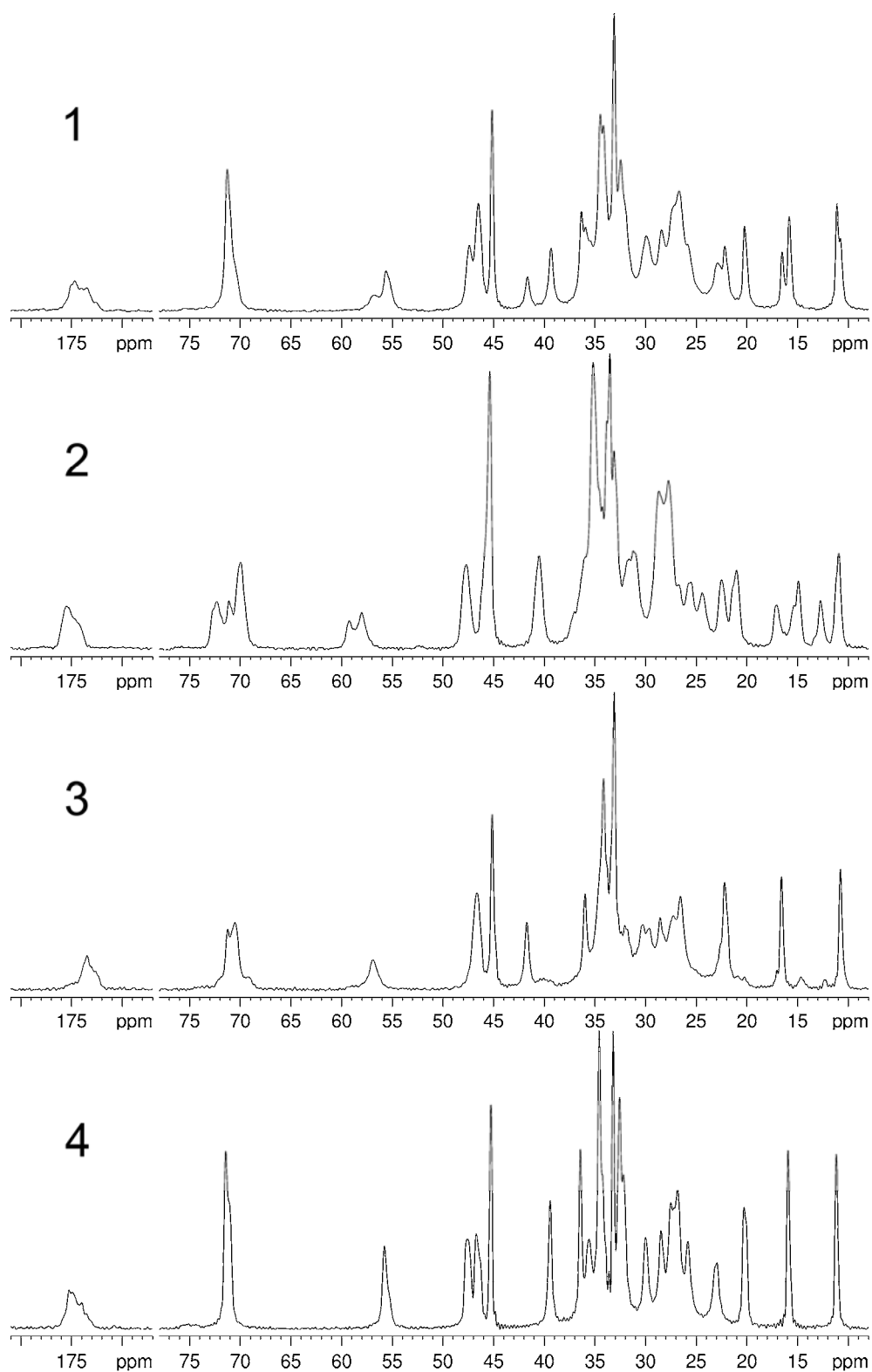
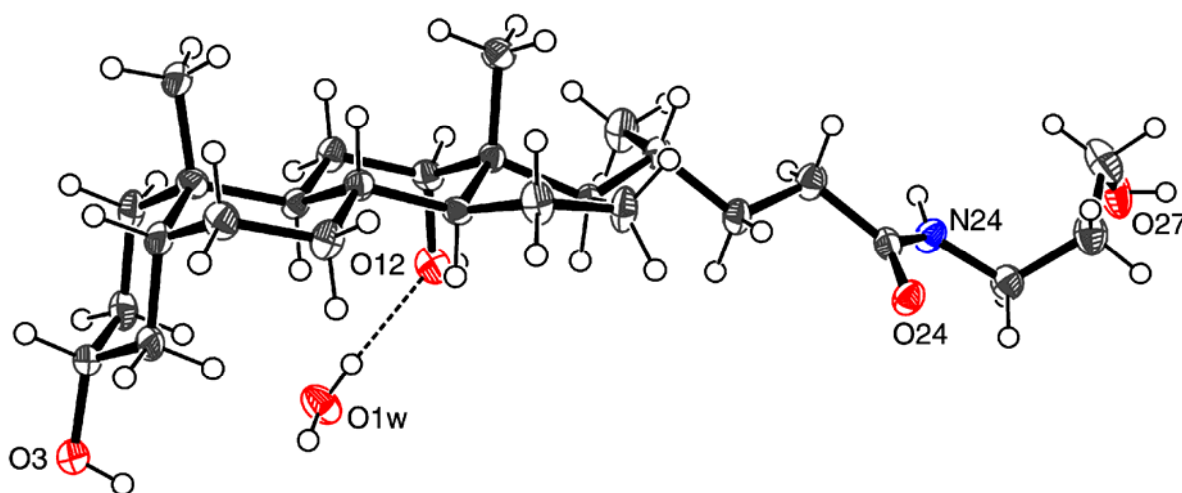
Figure 1. ^{13}C -CP/MAS-NMR spectra of solids 1–4.

Table 1. Selected chemical shifts in solid state ^{13}C CP/MAS NMR of 1-4.

C	1 ^a	2	3	4
3	71.3 ^c	71.1 ^d 70.0 ^d	70.5 ^d	71.4 ^c
12	71.3 ^c	72.3 ^d	71.2 ^d	71.4 ^c
18	11.1 10.8	12.7 10.9	10.8	11.2
19	22.2 20.2	22.5 21.0	22.2	20.3
21	16.5 15.8	17.0 14.9	16.6	15.9
24 ^b	174.7 173.5	175.5	173.5	175.2
27	56.8 55.6	59.2 58.0	56.9	55.8

^a1 is composed of forms 3 and 4; ^bC24 shows multiple resonances in all forms, only the most intensive one presented for 2-4; ^cC3 and C12 resonances overlapped (one singlet); ^dassignments can be interchanged.

The quality of the crystals of 3 was not very high, which can be observed from the refinement parameters (see Experimental section). Still, the structure was easily solved, although the internal consistency was poor. The selected asymmetric unit is presented in Figure 2.

Figure 2. Asymmetric unit of monohydrate 3. Thermal ellipsoids with 50 % probability level.

As can be seen from Figure 3, each water molecule is located in a hydrophilic “pocket”, formed by bile acid backbones. The hydroxyl groups of the bile acids are oriented to the same spatial direction creating a hydrophilic side for the molecule. When the molecules interact, these sides tend to turn towards each other and, thus building a pocket-like assembly. In this pocket a water molecule can easily be connected to the bile acid molecules, with three hydrogen bonds (Table 2); one visible in the asymmetric unit (Figure 2). While the anhydrous compound 4 has a hydrogen bond between O27 and

O24 [5], the structure of **3** does not contain any intramolecular hydrogen bonds. The terminal OH of the amidoalcohol side chain is instead hydrogen-bonded to O3 of the next bile acid molecule, forming a “head-to-tail” catenary architecture. The most interesting structure parameters of **3** are collected in Table 3, with the corresponding values of **4** for comparison.

Table 2. Hydrogen bond lengths (Å) and angles (°) of **3**.

D—H ... A	D—H	H ... A	D ... A	D—H ... A
O1 _w —H1 _{wb} ... O12	0.85(2)	2.00(2)	2.837(6)	172(7)
O3—H3 _O ... O24 ^a	0.84(2)	2.11(3)	2.932(5)	165(6)
O1 _w —H1 _{wa} ... O24 ^a	0.84(2)	2.07(2)	2.908(5)	176(7)
O12—H12 _O ... O27 ^b	0.84(2)	1.95(2)	2.773(6)	168(6)
N24—H24 ... O1 _w ^c	0.90(2)	2.06(2)	2.960(6)	174(5)
O27—H27 _O ... O3 ^d	0.83(2)	1.97(2)	2.791(6)	169(7)

Symmetry codes: (a) $\frac{1}{2} - x, 1 - y, \frac{1}{2} + z$; (b) $\frac{3}{2} - x, 1 - y, \frac{3}{2} + z$; (c) $\frac{3}{2} - x, 1 - y, -\frac{1}{2} + z$; (d) $x, y, -1 + z$.

Figure 3. Packing diagram of **3** with cell axes. The size of H₂O molecules is emphasized.

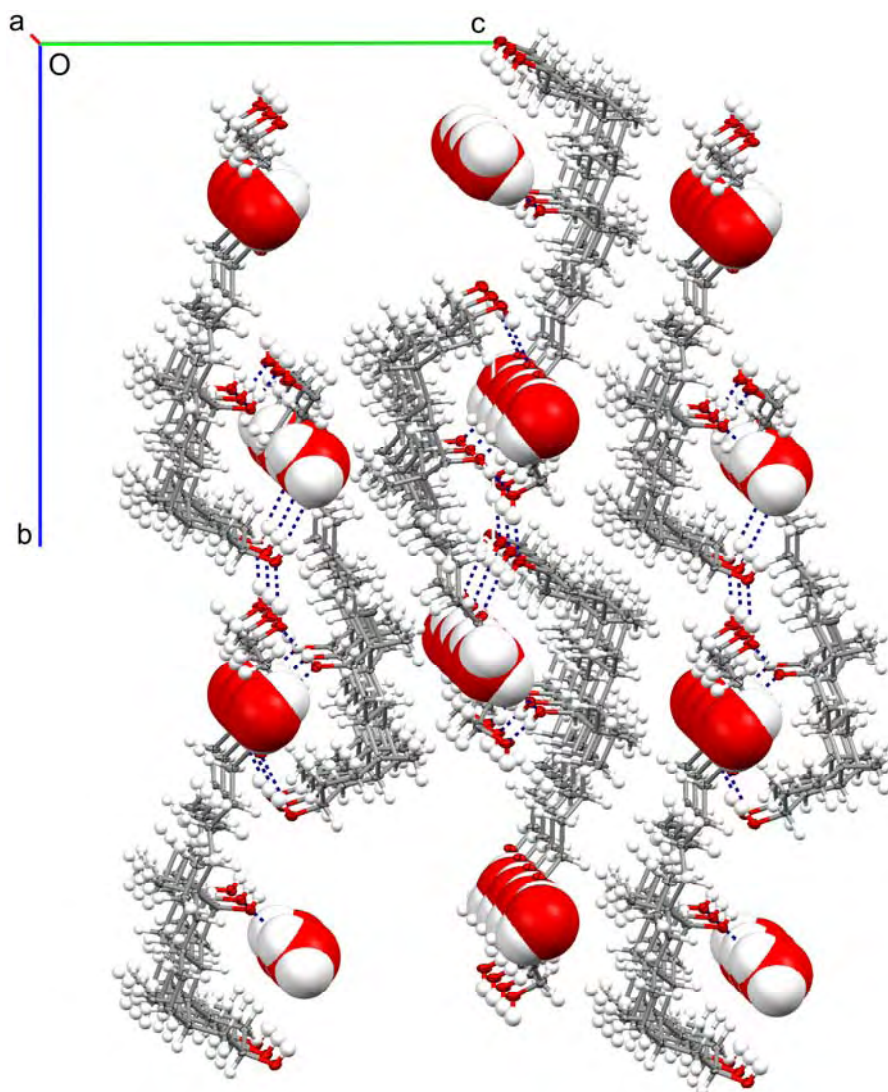
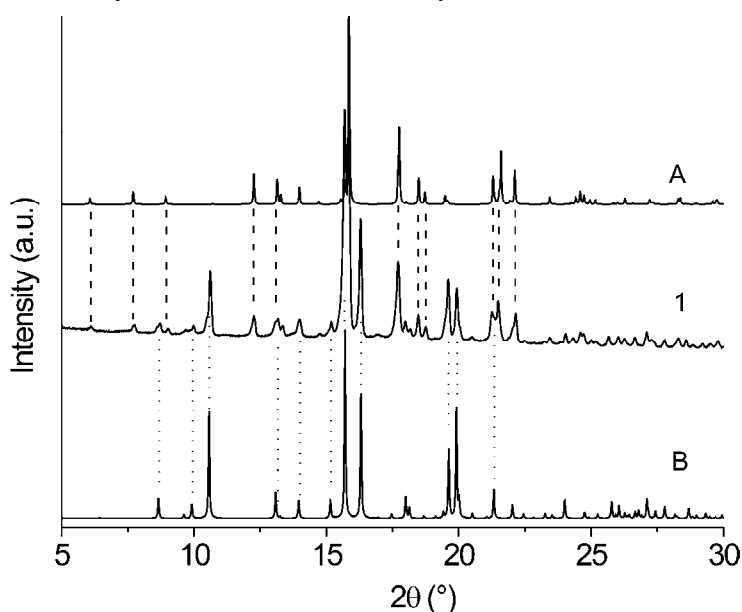


Table 3. Selected geometric parameters (Å, °) of **3** and **4** [5].

	3	4		3	4
C3 – O3	1.434(5)	1.444(3)	C20–C22–C23	115.4(4)	113.1(2)
C12 – O12	1.443(5)	1.433(3)	C22–C23–C24	113.3(4)	112.7(2)
C24 – O24	1.237(5)	1.244(3)	C23–C24–N24	114.4(4)	116.4(2)
C27 – O27	1.428(5)	1.422(4)	C24–N24–C25	123.3(4)	123.7(2)
C24 – N24	1.329(5)	1.332(3)	N24–C25–C26	113.4(4)	112.8(2)
C25 – N24	1.445(6)	1.459(3)	C25–C26–C27	113.5(4)	113.5(2)
C17 – C20	1.535(6)	1.534(3)	C26–C27–O27	111.8(4)	112.7(2)
C20 – C22	1.542(6)	1.537(3)			
C22 – C23	1.517(5)	1.524(3)	C17–C20–C22–C23	-178.1(4)	-172.3(2)
C23 – C24	1.516(6)	1.505(4)	C20–C22–C23–C24	177.6(4)	177.1(2)
C25 – C26	1.523(6)	1.521(4)	C22–C23–C24–N24	152.3(4)	122.5(3)
C26 – C27	1.504(6)	1.524(4)	C23–C24–N24–C25	175.3(4)	-174.8(2)
			C24–N24–C25–C26	-95.5(5)	-97.7(3)
			N24–N25–C27–C27	-71.5(5)	59.5(3)
			C25–C26–C27–O27	-66.2(5)	55.4(3)

The experimental powder diffraction patterns of the pseudopolymorphs **3** and **4** were compared to the simulated patterns that were generated from the known single crystal structure parameters. For the previously reported mixture (**1**) [5] the phase is clearly composed of two components that are consistent with single crystal structures found for anhydrous (**4**, simulated pattern **A**) and monohydrate (**3**, simulated pattern **B**) forms of *N*-(3-hydroxypropyl) 3 α ,12 α -dihydroxy-5 β -cholan-24-amide, as can be seen in Figure 4. The weight fraction of the phases is approx. 8:2 in favor of the anhydrous form (estimated by the TG analysis).

Figure 4. Experimental powder diffraction pattern of the previously reported polymorph mixture (**1**) [5], compared with the simulated powder patterns generated from the single crystal structures of anhydrous (**4**, **A**) and monohydrate (**3**, **B**) forms.



The samples of the anhydrous and monohydrate forms **4** and **3**, which we were able to crystallize as pure phases, as well as the solid **2** were compared to the simulated powder patterns **A** and **B**. The solid (**3**) crystallized from ethanol/water solution afforded pure monohydrate form, as can be seen in Figure 5. The powder pattern of the solid (**2**) is not congruent with **A** or **B**. This observation supports the NMR results presented above, and proves that slight variations in synthetic conditions resulted in a new polymorphic form. The anhydrous solid sample of (**4**) crystallized from acetonitrile (or *p*-xylene) is identical to the single crystal structure, as can be seen as a perfect consistency between the experimental and simulated powder patterns in Figure 6.

Figure 5. Experimental powder diffraction patterns of the new hydrate and monohydrate forms **2** and **3**, compared with the simulated powder pattern **B** generated from the single crystal structure of monohydrate form **3**.

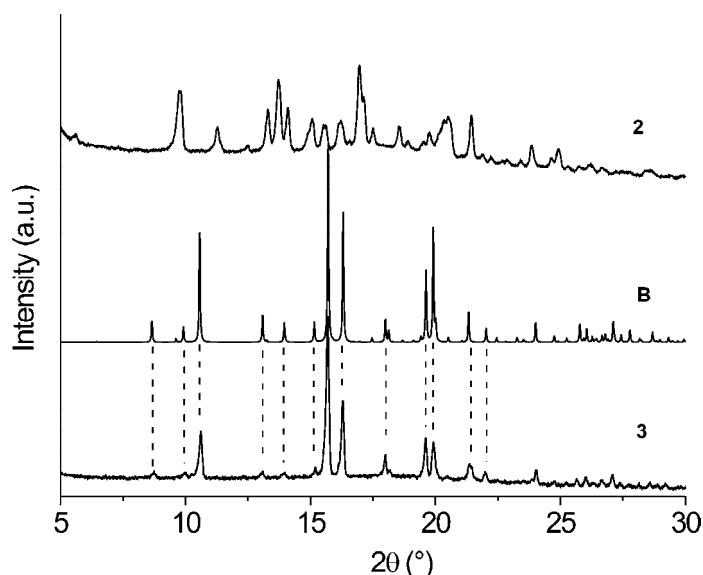
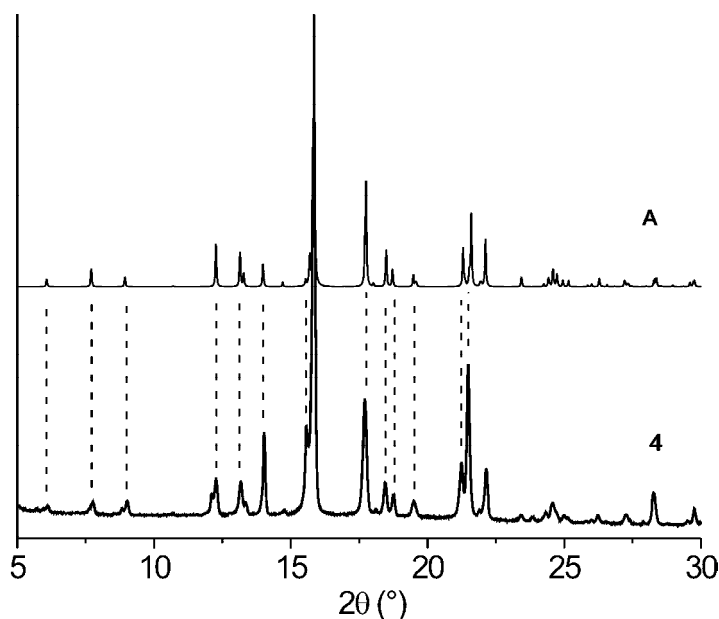


Figure 6. Experimental powder diffraction pattern of the anhydrous form **4** compared with the simulated powder pattern **A** generated from the single crystal structure.



The thermal behavior of each of the solids **1–4** was examined by TG/DTA and DSC. The results are summarized in Table 4 and the TG, DTA, and DSC curves are presented in Figures 7 and 8. The previously reported solid **1**, that proved to be a mixture of **3** and **4**, showed concurrent dehydration and melting of the monohydrate form, and furthermore, subsequent recrystallization to the anhydrous form **4**, which melting transition was finally observed at 179 °C. The observed melting temperature is consistent with the previously reported melting point for **1** (178.5–179.5 °C [5]). The solids of the two structurally different forms **2** and **3** showed also concurrent melting and dehydration transitions having onsets at ~115–116 °C. Typically, dehydration of solid **2** initiated somewhat at lower temperatures (40–50 °C) than on solid **3**, for which dehydration initiated at ~80–90 °C, as can be seen in Figure 8. This can also be seen from the TG curves (Figure 7), where the weight loss corresponding to dehydration on **2** is clearly more gradual than on **3**. Separate melting transitions for both hydrate forms were attempted to obtain by using a faster heating rate and hermetically sealed pans to prevent the initiation of dehydration. The resulted melting onsets for both of the hydrates were rather close to each other being 139 °C and 143 °C for **2** and **3**, respectively (Table 4). Consequent crystallization transition to the anhydrous form **4** was observed readily after dehydration of the monohydrate **3**. The same event was observed only occasionally on **2**, typically if slow heating rates were used. Probably in the case of the clearly more crystalline monohydrate **3**, the remaining seeds for further crystallization are more likely available on the dehydration/melting than on the less crystalline hydrate **2**. The anhydrous solid **4** showed only a single melting transition at 179 °C. In all cases, only the glass transition at 82 °C was observed on the second heating scan. The same phenomenon was also observed, if the first heating scan was ended after the dehydration transition, confirming concurrent dehydration and melting.

Table 4. The phase transition temperatures, their enthalpy changes and decomposition temperatures of solids **1–4**.

Comp.	1 st Heating $T_m, T_{dh}, T_c, (\Delta H): ^\circ\text{C}, (\text{J g}^{-1})$ $T_g, [\Delta C_p]: ^\circ\text{C}, [\text{J g}^{-1} ^\circ\text{C}^{-1}]$	2 nd heating $T_g, [\Delta C_p]:$ $^\circ\text{C}, [\text{J g}^{-1} ^\circ\text{C}^{-1}]$	Dec. $T_d: ^\circ\text{C}$
1	$T_{dh} + T_m$ 110.1 (30.92) T_c 135.5 (-5.17) T_m 179.0 (98.05)	T_g 81.6 [0.52]	321
2	$T_{dh} + T_m$ 116.3 (88.16) { T_m of hydrate 142.7}	T_g 80.1 [0.56]	323
3	$T_{dh} + T_m$ 115.4 (147.78) T_c 144.0 (-35.97) T_m 178.7 (88.51) { T_m of hydrate 139.4}	T_g 82.5 [0.58]	313
4	T_m 179.2 (96.12)	T_g 81.5 [0.49]	326

T_m = melting, T_g = glass-transition, T_c = crystallization, T_{dh} = dehydration, ΔC_p = change of heat capacity.

Figure 7. TG and DTA curves for the solids **1-4** measured with heating rate of $10\text{ }^{\circ}\text{C min}^{-1}$.

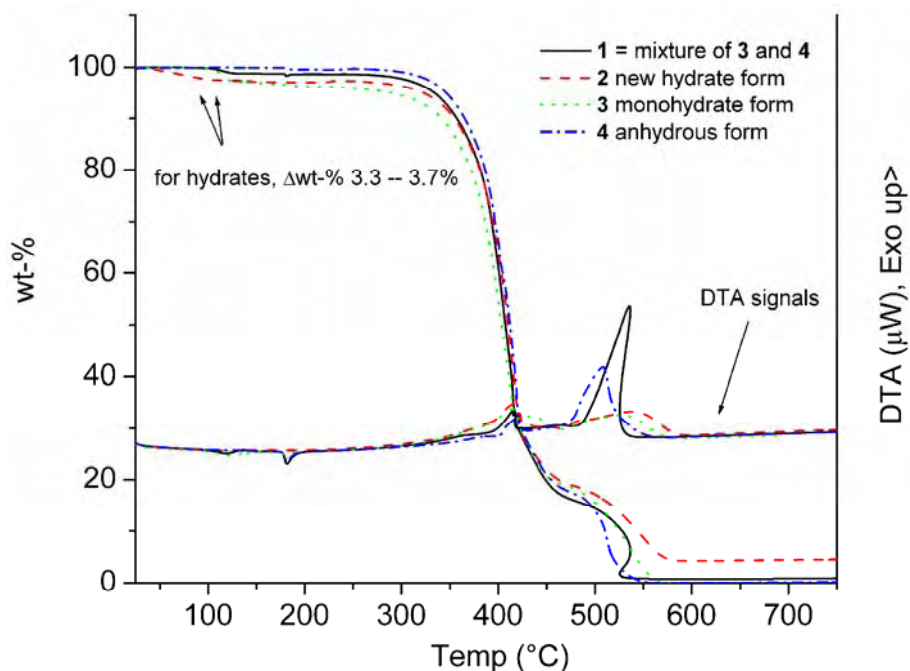
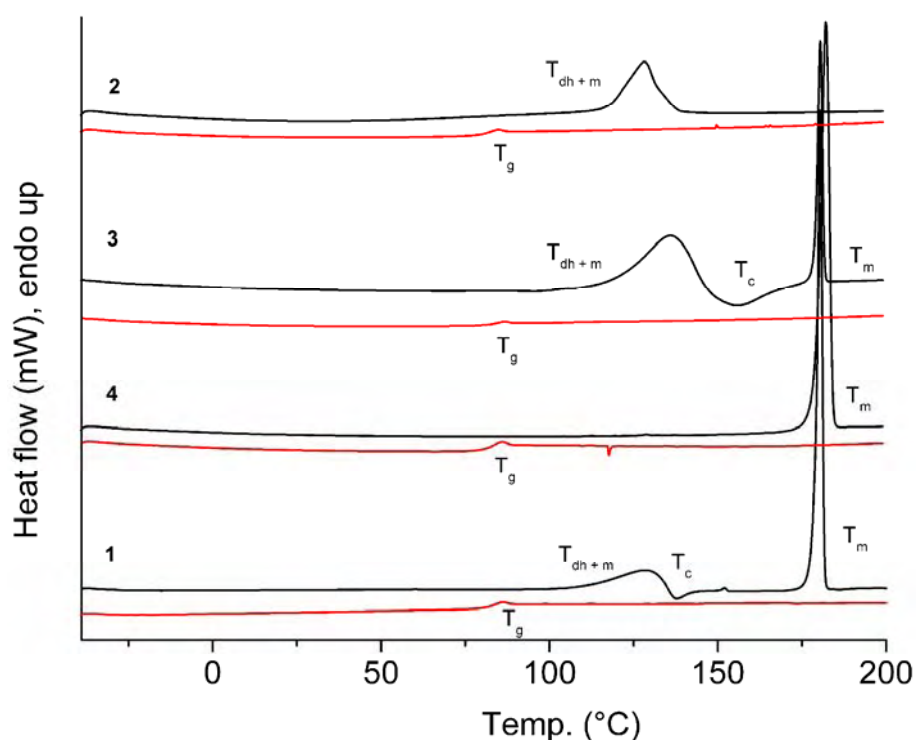


Figure 8. DSC scans of solids **1-4**. On each pair of scans: first heating scan is on top.



As all the examined solids dehydrated and/or melted before starting to decompose, being consistent with the anhydrous form **4** in that respect, a common decomposition temperature was obtained for all of the solids at $\sim 320\text{ }^{\circ}\text{C}$. In addition, both hydrate forms, **2** and **3**, showed weight losses corresponding to dehydration. For the known monohydrate **3**, the weight loss of $\sim 4.0\%$, which agrees well with a theoretical wt-% of 3.8%, was obtained. Nearly similar wt-% of 3.3–3.7% were obtained from sample

to sample for the second hydrate form **2**, suggesting that its composition seems to be close to that of stoichiometric monohydrate. As can be seen in the powder diffraction pattern (Figure 5), however, the molecular packing is different, which in part may be due to insufficient packing of water in the lattice (due to fast crystallization). The crystallinity of **2** is lower than that of **3**.

It has been reported in the literature [30] that the side chain of a bile acid can usually exist in two conformations defined by the dihedral angle of the side chain at C17-C20-C22-C23. In the *trans* conformation this angle varies approximately between 160° and 180°, whereas the *gauche* form possesses values of the dihedral angle ranging roughly from 60° to 70°. The angles in the single crystal structures of **3** and **4** (Table 3) were -178.1(4)° and -172.3(2)°, respectively, establishing *trans* conformation. The same is true for the HF/6-31G*-optimized structures of **3** and **4**, for which the corresponding values were -172.1° and -172.7°, respectively. The selected calculated ¹³C-NMR chemical shifts for the optimized structures are presented in Table 5 with the corresponding experimental data. The largest deviations between the calculated ¹³C-NMR chemical shifts of these two pseudopolymorphs can be observed for the side chain carbons, namely C24, C26, and C27, due to different geometries of the side chains. This is more or less in agreement with the experimental data. The differences between the exact values of the calculated and experimental shifts are probably due to the fact that the shifts are calculated for single molecules in vacuo. The method thus excludes intermolecular interactions between the bile acid molecules. Inclusion of more than one bile acid molecule in the calculation at this level would, however, have unreasonably increased the CPU time needed for the calculations.

Table 5. Selected theoretical (B3LYP/6-311G*) and experimental ¹³C NMR parameters calculated and measured for **3** and **4**.

C	$\delta_{\text{theor}} \mathbf{3}$	$\delta_{\text{theor}} \mathbf{4}$	$\delta_{\text{exp}}(\text{solid}) \mathbf{3}$	$\delta_{\text{exp}}(\text{solid}) \mathbf{4}$	$\delta_{\text{exp}}(\text{CDCl}_3) \mathbf{1}$
3	71.57	73.77	70.5	71.4	71.89
12	77.23	75.71	71.2	71.4	73.24
18	11.51	11.41	10.8	11.2	12.81
19	21.26	22.45	22.2	20.3	23.18
21	16.85	16.47	16.6	15.9	17.54
24	168.15	171.83	173.5	175.2	174.58
27	59.86	57.35	56.9	55.8	59.70

The current findings show that our previous report of **1** [5] was not fully accurate. The gelation ability of **1** were erroneously considered to be only caused by pure *N*-(3-hydroxypropyl)-3 α ,12 α -dihydroxy-5 β -cholan-24-amide (**4**). Now, when **1** is proved to be a mixture of forms **3** and **4**, the gelation ability must be actually a co-operative action of these two pseudopolymorphs. We tested quickly the gelation of chlorobenzene with **3** and **4** and observed no gelation at all, which confirms the co-operative nature. Review of these results suggests that the synthetic procedures in general result in the monohydrate, although in the powdery solid **1** the anhydrous form is predominant. The reason why three different solids were obtained with similar synthetic routes (exactly identical for **1** and **3**) and why **2** is different from the other solids still remain ambiguous to us.

Conclusions

Four different solid materials containing *N*-(3-hydroxypropyl) 3 α ,12 α -dihydroxy-5 β -cholan-24-amide were structurally characterized. Solid **1** was previously characterized to contain two phases, from which the main component was identified to be anhydrous *N*-(3-hydroxypropyl)3 α ,12 α -dihydroxy-5 β -cholan-24-amide [5] (form **4**) and the structural form of the minor phase remained unknown. In this study the minor component of the mixture was identified to be a monohydrate form **3**, thus solid **1** being a mixture of forms **3** and **4**. Solid **2** was also found to be a monohydrate, identified as a polymorph of **3**. The exact structure of form **2** remained unknown. The monohydrate **3** is obtained either by a direct synthesis or by recrystallization of any of the powdery solids (**1-3**) from water/ethanol (2:1) mixture. The anhydrous solid **4** was obtained by recrystallization of the powdery solids (**1-3**) from acetonitrile or *p*-xylene. The monohydrate **3** does not contain an intramolecular hydrogen bond, found in its pseudopolymorph **4** between O27 and O24. The structural characterization of polymorphs and pseudopolymorphs of *N*-(hydroxyalkyl) amides, as well as the other bile acid derivatives, are one of the primary interests of our research group. More results from different *N*-(hydroxyalkyl) amides are to come in the near future.

Experimental Section

Compounds

The first synthetic procedure for preparing *N*-(3-hydroxypropyl) 3 α ,12 α -dihydroxy-5 β -cholan-24-amide (Scheme 1) with 5 days of reaction time in rt. resulted in white powdery solid **1**, described in [5]. In the second procedure the reaction mixture was refluxed for 65 h and resulted in white solid **2** as well, but with a much better yield (79 %, compared to 37 % reported in [5]). Solid **2** was identified as *N*-(3-hydroxypropyl)-3 α ,12 α -dihydroxy-5 β -cholan-24-amide monohydrate. Identical solid **2** was also obtained at room temperature with the same reaction time. A third different solid **3** was obtained when the first synthetic procedure was repeated. Only this time the precipitate from water was different from **1** and **2**. This *N*-(3-hydroxypropyl)-3 α ,12 α -dihydroxy-5 β -cholan-24-amide monohydrate was also obtained by recrystallization of whichever of the powdery solids (**1-3**) from a 2:1 mixture of water and ethanol. For analytical studies the samples of **3** were prepared by recrystallization. Pure crystals of anhydrous *N*-(3-hydroxypropyl)-3 α ,12 α -dihydroxy-5 β -cholan-24-amide (**4**) were obtained by recrystallization of the powdery solids **1-3** from acetonitrile or *p*-xylene. The solid **1** was found to be a mixture of **3** and **4**. All organic solvents used were of analytical grade and water was deionized before use.

Spectroscopy

Liquid state NMR characterization results of **1** have been presented previously [5]. All ¹³C-CP/MAS measurements were performed at room temperature with Bruker Avance 400 MHz NMR spectrometer, equipped with a 4 mm standard bore CP/MAS probehead, using 4 mm zirconia rotors. The samples were spun at 10 kHz. The CP contact time was 4 ms and relaxation delay 5 s. For chemical shift calibration the spectrum of glycine sample, with known chemical shifts (173.3 and

42.6), was measured prior to bile acid sample. The complete lists of NMR acquisition and processing parameters are available from E.K. on request. IR absorption spectra were recorded with Mattson Satellite FTIR spectrometer, using KBr disc method.

Thermal properties

The thermal decompositions of the compounds were examined with Perkin-Elmer PYRIS DIAMOND TG/DTA thermogravimetric analyzer. The measurements were carried out in open platinum pans under a synthetic air atmosphere (a flow rate of 150 ml min⁻¹) with a heating rate of 10 (or 20) °C min⁻¹ at a temperature range of 25–700 (or 900) °C. The temperature calibration of the TG/DTA was made by using the melting points of five reference materials (In, Sn, Zn, Al, Au). The weight balance was calibrated by measuring a standard weight as a function of temperature. The sample weights used in the measurements were 4–10 mg.

Thermal behavior of the compounds was determined on power compensation type Perkin-Elmer PYRIS DIAMOND DSC. The measurements were carried out under nitrogen atmosphere (flow rate 50 ml min⁻¹) using 50 µl sealed aluminum sample pans. The sealing was made by using a 30 µl aluminum pan with capillary holes to ascertain good thermal contact between the sample and the pan, and to minimize the free volume inside the pan. Some measurements were also performed with hermetically 50 µl sealed aluminum sample pans to investigate the melting transitions of the hydrate forms. The temperature calibration was made using two standard materials (n-decane, In) and energy calibration by an indium standard (28.45 J g⁻¹). Typically, following temperature profile was used for each sample: a sample was heated from -40 to ~20–30 °C above the predetermined melting transition with a heating rate of 10 °C min⁻¹, followed by one minute hold at the end temperature, and cooled down to -40 °C with a rate of 10 °C min⁻¹. The heating-cooling cycle was repeated once and the sample was held at -40 °C for 5 min before initiation of the next cycle. Single heating scans from 25 to 160 °C with a rate of 20 °C min⁻¹ were made to obtain melting transition for the hydrate forms. The melting (T_m), crystallization (T_c), dehydration (T_{dh}), and decomposition (T_d) temperatures were obtained as extrapolated onsets. The glass transition temperature (T_g) was obtained at half-step temperature of ΔC_p change. Uncertainty for measured temperatures was less than 0.7 °C for all measurements. Sample weights of 2.5–6 mg were used on the measurements. The sample weight was checked afterwards to monitor a weight loss that may have occurred during the scans.

X-ray powder diffraction analysis

The x-ray powder diffraction data were obtained at room temperature by the Huber imaging-plate Guinier camera 670 using germanium monochromatized CuK_{α1} radiation ($\lambda = 1.5406 \text{ \AA}$; 45 kV, 25 mA). The measurements were carried out in Guinier-type transmission geometry with the angle of incidence 45° to the sample normal. The hand-ground samples were prepared on the paraffin-coated Mylar foil of 3.5 µm thickness, which was mounted on vertical sample holder oscillating horizontally. The x-ray diffraction data were recorded with a curved, position sensitive imaging plate detector using 2θ-angle range of 4–100° and step resolution of 0.005°. The recording times were sample dependent varying typically from 20 to 300 min. The simulated powder diffraction patterns were calculated with

MERCURY [31] from the single crystal structures (CIF) of forms **3** and **4**, and are labeled further on as (**B**) and (**A**), respectively.

X-ray single crystal diffraction analysis [32]

The structure of *N*-(3-hydroxypropyl) 3 α ,12 α -dihydroxy-5 β -cholan-24-amide (**4**) was reported earlier by us [5]. The x-ray structural data of *N*-(3-hydroxypropyl) 3 α ,12 α -dihydroxy-5 β -cholan-24-amide monohydrate form **3**, crystallized from water/ethanol (2:1), was collected with Bruker-Nonius Kappa APEX-II diffractometer at 173.0 \pm 0.1 K using graphite monochromatized MoK α radiation (λ = 0.71073 Å) and COLLECT [33] data collection software. Data was processed with DENZO-SMN [34]. The structure was solved by direct methods, using SIR2002 [35], and refined on F^2 , using SHELXL-97 [36] in WinGX [37] program package. The reflections were corrected for Lorentz polarization effects and absorption correction was not used. The hydrogen atoms, except N-H and O-H, were calculated to their idealized positions with isotropic temperature factors (1.2 or 1.5 times the C temperature factor) and refined as riding atoms. Hydrogens attached to N or O were found from electron density maps and fixed to their ideal distance from their parent atoms (0.91 Å for N-H and 0.84 Å for O-H at 173 K), with isotropic temperature factors (1.2 or 1.5 times the parent atom factor). The figures were drawn with ORTEP-3 [38] and MERCURY [31]. Other experimental x-ray data are shown in Table 6.

Table 6. Crystal data and structure refinement of **3**.

Empirical formula	C ₂₇ H ₄₉ NO ₅
Formula weight	467.67
Temperature (K)	173
Wavelength (Å)	0.71073
Crystal system	Orthorhombic
Space group	<i>P</i> 2 ₁ 2 ₁ 2 ₁
Unit cell dimensions (Å)	<i>a</i> = 7.1151(2) <i>b</i> = 18.1803(4) <i>c</i> = 20.1803(5)
Volume (Å ³)	2610.42(11)
<i>Z</i>	4
Density _{calc} (Mg/m ³)	1.190
Absorption coefficient (mm ⁻¹)	0.080
<i>F</i> (000)	1032
Crystal size (mm)	0.30 × 0.10 × 0.10
Index ranges	-8 ≤ <i>h</i> ≤ 8; -21 ≤ <i>k</i> ≤ 21; -23 ≤ <i>l</i> ≤ 23
Reflections collected/unique	17693/2649 [<i>R</i> _{int} = 0.1650]
Data/restraints/parameters	2649/6/319
Goodness-of-fit on F^2	1.070
Final <i>R</i> indices [<i>I</i> > 2σ(<i>I</i>)]	<i>R</i> ₁ = 0.0595; w <i>R</i> ₂ = 0.0960
<i>R</i> indices (all data)	<i>R</i> ₁ = 0.0870; w <i>R</i> ₂ = 0.1062
Largest diff. peak and hole (eÅ ⁻³)	0.202 and -0.227

Molecular modeling

The NMR chemical shifts for crystallized forms **3** and **4** were calculated with DFT B3LYP/6-311G* level of theory using gauge independent atomic orbital (GIAO) [39] method by Gaussian98 software [40]. The single crystal structure was first optimized using molecular mechanics (MM+ force field) [41] and semiempirical PM3 method [42] with HyperChem molecular modeling software [43]. Finally, the structure was forwarded for geometry optimization at *ab initio* HF/6-31G* level of theory in Gaussian98 package. The NMR chemical shifts were then calculated for the optimized structures. The complete list of the calculated shifts for forms **3** and **4** can be obtained from authors on request.

Acknowledgements

E.S. gratefully acknowledges financial support from Academy of Finland (project no. 7105950). V.N. wishes to thank the Finnish Society of Sciences and Letters, the Foundation of Magnus Ehrnrooth, for funding.

References and Notes

1. Davis, A.P. Cholaphanes et al.; steroids as structural components in molecular engineering. *Chem. Soc. Rev.* **1993**, *22*, 243-253.
2. Enhsen, A.; Kramer, W.; Wess, G. Bile acids in drug discovery. *Drug Discov. Today* **1998**, *3*, 409-418.
3. Yoswathananont, N.; Miyata, M.; Nakano, K.; Sada, K. *Perspectives in Supramolecular Chemistry*; Toda, F.; Bishop, R. (Eds.); Wiley: New York, **2004**; Vol 8, *Separations and Reactions in Organic Supramolecular Chemistry*, pp. 87-122 and references cited therein.
4. Bortolini, O.; Fantin, G.; Fogagnolo, F. Bile acid derivatives as enantiodifferentiating host molecules in inclusion processes. *Chirality* **2005**, *17*, 121-130 and references cited therein.
5. Valkonen, A.; Lahtinen, M.; Virtanen, E.; Kaikkonen, S.; Kolehmainen, E. Bile acid amidoalcohols: simple organogelators. *Biosens. Bioelectron.* **2004**, *20*, 1233-1241.
6. Willemen, H.M.; Vermonden, T.; Marcelis, A.T.M.; Sudhölter, E.J.R. *N*-Cholyl amino acid alkyl esters - a novel class of organogelators. *Eur. J. Org. Chem.* **2001**, 2329-2335.
7. Willemen, H.M.; Vermonden, T.; Marcelis, A.T.M.; Sudhölter, E.J.R. Alkyl Derivatives of Cholic Acid as Organogelators: One-Component and Two-Component Gels. *Langmuir* **2002**, *18*, 7102-7106.
8. Sangeetha, N.M.; Balasubramanian, R.; Maitra, U.; Ghosh, S.; Raju, A.R. Novel Cationic and Neutral Analogues of Bile Acids: Synthesis and Preliminary Study of Their Aggregation Properties. *Langmuir* **2002**, *18*, 7154-7157.
9. Babu, P.; Sangeetha, N.M.; Maitra, U. Supramolecular chemistry of bile acid derivatives: formation of gels. *Macromol. Symp.* **2006**, *241*, 60-67 and references cited therein.
10. Terech, P.; Sangeetha, N.M.; Maitra, U. Molecular Hydrogels from Bile Acid Analogues with Neutral Side Chains: Network Architectures and Viscoelastic Properties. Junction Zones, Spherulites, and Crystallites: Phenomenological Aspects of the Gel Metastability. *J. Phys. Chem.* **2006**, *B110*, 15224-15233.

11. Mukhopadhyay, S.; Maitra, U.; Ira; Krishnamoorthy, G.; Schmidt, J.; Talmon, Y. Structure and Dynamics of a Molecular Hydrogel Derived from a Tripodal Cholamide. *J. Am. Chem. Soc.* **2004**, *126*, 15905-15914.
12. Maitra, U.; Babu, P. First synthesis of phosphonobile acids and preliminary studies on their aggregation properties. *Steroids* **2003**, *68*, 459-463.
13. Harris, R.K. NMR crystallography. The use of chemical shifts. *Solid State Sci.* **2004**, *6*, 1025-1037.
14. Harris, R.K.; Cadars, S.; Emsley, L.; Yates, J.R.; Pickard, C.J.; Jetti, R.K.R.; Griesser, U.J. NMR crystallography of oxybuprocaine hydrochloride, Modification II^o. *Phys. Chem. Chem. Phys.* **2007**, *9*, 360-368.
15. Bowles, R.K.; Morgan, K.R.; Furneaux, R.H.; Coles, G.D. ¹³C CP/MAS NMR study of the interaction of bile acids with barley β-D-glucan. *Carbohydr. Polym.* **1996**, *29*, 7-10.
16. Hoagland, P.D.; Pfeffer, P.E. Cobinding of bile acids to carrot fiber. *J. Agric. Food Chem.* **1987**, *35*, 316-319.
17. Heyes, S.J.; Dobson, C.M. Carbon-13 CP/MAS NMR study of the inclusion polymerization of 2,3-dimethylbutadiene in deoxycholic acid. *Macromolecules* **1992**, *25*, 3617-3623.
18. Nakaoki, T.; Sumida, T.; Takagi, M.; Takemoto, K. High resolution solid state ¹³C NMR investigation of the deoxycholic acid/ferrocene inclusion compound. *Polym. Bull.* **1999**, *43*, 365-369.
19. Imashiro, F.; Kuwahara, D.; Terao, T. Carbon-13 solid-state NMR study on populations, conformations, and molecular motions of γ-valerolactone enantiomers enclathrated in the chiral cholic acid host. *J. Chem. Soc. Perkin Trans. 2* **1993**, 1759-1763.
20. Nakamura, S.; Imashiro, F.; Takegoshi, K.; Terao, T. Sequential Arrangement of γ-Valerolactone Enantiomers Enclathrated in Cholic Acid Channels as Studied by ¹³C Solid-State NMR: Elucidation of the Optical Resolution Mechanism. *J. Am. Chem. Soc.* **2004**, *126*, 8769-8776.
21. Hazra, B.G.; Pore, V.S.; Dey, S.K.; Datta, S.; Darokar, M.P.; Saikia, D.; Khanuja, S.P.S.; Thakur, A.P. Bile acid amides derived from chiral amino alcohols: novel antimicrobials and antifungals. *Bioorg. Med. Chem. Lett.* **2004**, *14*, 773-777.
22. Mosbach, E.H.; Ayengar, N.K.N.; McSherry, C.K. Synthesis of steroid compounds. *U.S. Pat. 4460509*, **1984**.
23. Mosbach, E.H.; McSherry, C.K.; Kuroki, S. Synthesis of 3α,12α-dihydroxy-7-methyl-5β-chol-6 and 7-en-24-oic acids and 7-methylene-5β-cholan-24-oic acid as intermediates for cholelithiasis therapeutics. *U.S. Pat. 4648995*, **1987**.
24. Della Valle, Fr.; Lorenzi, S.; Samson, J.C.J.J.; Della Valle, Fe. Pharmaceutical compositions containing N-acyl derivatives of aminoalcohols for the treatment of pathologies involving mast cells. *Eur. Pat. Appl. EP 0550006*, **1993**.
25. Della Valle, Fr.; Lorenzi, S.; Samson, J.C.J.J.; Della Valle, Fe. N-Acyl derivatives of amino alcohols active as local autacoids and useful in the therapy of autoimmune processes. *U.S. Pat. 5506224*, **1996**.
26. Della Valle, Fr.; Lorenzi, S.; Della Valle, Fe. Aminoalcohol N-acyl derivatives as therapeutic agents against the neurogenic endoneural edema of the peripheral nerve. *U.S. Pat. Appl. US 5679667*, **1997**.

27. Bundy, R.; Mauskopf, J.; Walker, J.T.; Lack, L. Interaction of uncharged bile salt derivatives with the ileal bile salt transport system. *J. Lipid Res.* **1977**, *18*, 389-395.
28. Mukai, A.; Yazawa, K.; Mikami, Y.; Harada, K.; Gräfe, U. Biotransformation of bile acids by pathogenic actinomycetes *Nocardia otitidiscaviarum* and *Amycolatopsis* sp. strains. *J. Antibiot.* **2005**, *58*, 356–360.
29. Cambridge Structural Database (CSD, Version 5.28); CCDC: Cambridge, UK, **2006**.
30. Nakano, K.; Sada, K.; Kurozumi, Y.; Miyata, M. Importance of packing coefficients of host cavities in the isomerization of open host frameworks: guest-size-dependent isomerization in cholic acid inclusion crystals with monosubstituted benzenes. *Chem. Eur. J.* **2001**, *7*, 209-220.
31. Macrae, C.F.; Edgington, P.R.; McCabe, P.; Pidcock, E.; Shields, G.P.; Taylor, R.; Towler, M.; van de Streek, J. *Mercury*: visualization and analysis of crystal structures. *J. Appl. Cryst.* **2006**, *39*, 453-457.
32. CCDC-635027 contains the supplementary crystallographic data for this paper. These data can be obtained free of charge via www.ccdc.cam.ac.uk/conts/retrieving.html (or from the CCDC, 12 Union Road, Cambridge CB2 1EZ, UK; fax: +44 1223 336033; e-mail: deposit@ccdc.cam.ac.uk)
33. *COLLECT*. Bruker AXS Inc.: Madison, WI, **2004**.
34. Otwinowski, Z.; Minor, W. *Methods in Enzymology*; Carter Jr., C.W.; Sweet R.M. (Eds.); Academic Press: New York, **1997**; vol. 276, *Macromolecular Crystallography*; Part A, pp. 307-326.
35. Burla, M.C.; Camalli, M.; Carrozzini, B.; Cascarano, G.L.; Giacovazzo, C.; Polidori, G.; Spagna, J. *SIR2002*: the program. *J. Appl. Cryst.* **2003**, *36*, 1103.
36. Sheldrick, G.M. *SHELXL-97*; University of Göttingen: Göttingen, Germany, **1997**.
37. Farrugia, L.J. *WinGX* suite for small-molecule single-crystal crystallography. *J. Appl. Cryst.* **1999**, *32*, 837-838.
38. Farrugia, L.J. *ORTEP-3* for Windows – a version of *ORTEP-III* with a Graphical User Interface (GUI). *J. Appl. Cryst.* **1997**, *30*, 565.
39. Wolinski, K.; Hinton, J.F.; Pulay, P.J. Efficient implementation of the gauge-independent atomic orbital method for NMR chemical shift calculations. *J. Am. Chem. Soc.* **1990**, *112*, 8251-8260.
40. Frisch, M.J.; Trucks, G.W.; Schlegel, H.B.; Scuseria, G.E.; Robb, M.A.; Cheeseman, R.E.; Zakrzewski, W.G.; Montgomery Jr., J.A.; Stratmann, R.E.; Burant, J.C.; Dapprich, S.; Millam, J.M.; Daniels, A.D.; Kudin, K.N.; Strain, M.C.; Farkas, O.; Tomasi, J.; Barone, V.; Cossi, M.; Cammi, R.; Mennucci, B.; Pomelli, C.; Adamo, C.; CliVord, S.; Ochterski, J.; Petersson, G.A.; Ayala, P.Y.; Cui, Q.; Morokuma, K.; Malick, D.K.; Rabuck, A.D.; Raghavachari, K.; Foresman, J.B.; Cioslowski, J.; Ortiz, J.V.; Stefanov, B.B.; Liu, G.; Liashenko, A.; Piskorz, P.; Komaromi, I.; Gomperts, R.; Martin, R.L.; Fox, D.J.; Keith, T.; AllLaham, M.A.; Peng, C.Y.; Nanayakkara, A.; Gonzalez, C.; Challacombe, M.; Gill, P.M.W.; Johnson, B.; Chen, W.; Wong, M.W.; Andres, J.L.; Head-Gordon, M.; Replogle, E.S.; Pople, J.A. *Gaussian 98; Revision A.9*; Gaussian: Pittsburg, PA, **1998**.
41. a) Allinger, N.L. Conformational analysis. 130. MM2. A hydrocarbon force field utilizing V_1 and V_2 torsional terms. *J. Am. Chem. Soc.* **1977**, *99*, 8127-8134; b) Allinger, N.L.; Yuh Y.H. *Quantum Chemistry Program Exchange*; Bloomington IN; Program No. 395; c) Burkert, U.; Allinger, N.L.

(Eds.), *Molecular Mechanics*; ACS Monograph 177; American Chemical Society: Washington, D.C., 1982.

42. Stewart, J.J.P. Optimization of parameters for semiempirical methods. I. Method. *J. Comput. Chem.* **1989**, *10*, 209-220.
43. *HyperChemTM*, Release 7.0 for Windows; Hypercube, Inc.: Gainesville, FL, 2002.

Sample Availability: Samples of the compounds **1** - **4** are available from authors.

© 2007 by MDPI (<http://www.mdpi.org>). Reproduction is permitted for noncommercial purposes.